Reptation Dynamics with Random Local Interactions

Sylvain J. Hubert, Martin Krzywinski, Ivan L'Heureux, and Gary W. Slater*

Department of Physics, University of Ottawa, 150 Louis-Pasteur, Ottawa, Ontario, Canada K1N 6N5

Received May 30, 1997; Revised Manuscript Received October 28, 1997

ABSTRACT: We generalize the reptation model to treat cases where the N segments of the primitive chain can interact with a static environment (such as a gel). The rates of tube segment renewal are calculated taking into account both an external field and local interaction energies. This model can be used, e.g., to study the migration of polymers in a random environments (where local entropic and elastic effects can play a role). We then present a study of polymer reptation in a tube with a random (annealed) energy landscape, similar to the one described by Lumpkin and Zimm. In particular, if an external field is applied, the predictions of the biased reptation model are modified. We find that for low field intensities, the electrophoretic mobility μ scales like $1/N^{1+\alpha}$ where the exponent $\alpha \geq 0$ increases with the strength of the random energies.

1. Introduction

The original reptation (or tube) model of de Gennes[1] and Doi and Edwards[2−5] was developed to understand the diffusion of linear polymers (e.g., polystyrene) in dense systems such as melts or gels. In this model, the disengagement time of a primitive chain made of N segments (tube sections) is predicted to scale like $\tau \sim N^3$ since the chain essentially undergoes a one-dimensional random-walk inside a three-dimensional topological tube of length $L \sim N$. The diffusion coefficient is then given by $D \sim (R_g)^2/\tau$, where $R_g \sim N^\nu$ is the radius-of-gyration of the polymer and ν is Flory's exponent. Since the excluded volume effects are screened in a melt, one has $\nu = {}^1/_2$, and the reptation model predicts $D \sim 1/N^2$ (for $N \gg 1$), a relation that has been tested extensively both experimentally[6] and in computer simulations[7]. In a gel, on the other hand, one would expect $\nu = {}^3/_5$ because of the absence of screening, and the model then predicts the slightly weaker dependency $D \sim 1/N^{9/5}$. Lodge and Rotstein[8] measured the diffusion coefficient of linear polystyrene in poly(vinyl methyl ether) gels using dynamic light scattering and found that $D \sim 1/N^{2+\alpha}$, with $\alpha = 0.7-0.8$, an exponent that certainly does not agree with the predictions of the reptation model.

One possible explanation for large (positive) values of α was suggested by the computer simulations of Baumgartner and Muthukumar.[9,10] These authors showed that when the mean "pore" size $\bar{a}$ of a quenched random medium (not a melt) is comparable to R_g, the polymer molecule prefers to reside into the largest pores of the system ($a > \bar{a} \cong R_g$) to maximize its entropy. Since these pores are connected by narrower channels of width $a < R_g$, the long-range motion of the polymers is through a hopping process where the channels act like "entropic barriers". The physics of this problem is similar to that of a particle moving in a system with a rough energy landscape.[11,12] The diffusion coefficient D then decreases very quickly with molecular size N; scaling arguments based on an energy barrier model in fact predict that the dependence should be exponential instead of power law.[13] However, if we fit simulation data with a power law (which often provides a good fit because the range of polymer molecular sizes accessible by computer simulations is fairly narrow), we find that the exponent α increases from about $1 - 2\nu \leq 0$ (for periodic arrays of obstacles) to values exceeding ${}^1/_2$ for very disordered environments.[13,14] Entropic trapping has therefore been invoked to explain anomalous diffusion data[8] showing large values of α. Recent computer simulations have demonstrated that entropic trapping disappears when the gel fibers stop forming a percolating cluster that limits the long-range diffusion of the polymer.[14]

Gel electrophoresis (GE) of polyelectrolytes is usually described by either the Ogston[17] or the biased reptation[18−20] model. For low electric fields, the Nernst−Einstein relationship $\mu/D \sim N+1$ should be satisfied, where μ is the electrophoretic mobility. Using the reptation relation $D \sim 1/N(N+1)$, this relationship predicts $\mu \sim 1/N$ in this limit, a prediction of the biased reptation model (BRM) that is in excellent agreement with a large body of experimental results for DNA GE.[18−20] Note, however, that large electric forces tend to bring the system far from equilibrium; both μ and D then become strongly field dependent while their molecular-size dependence is greatly reduced (this is due to the alignment of the molecule along the field direction). Not surprisingly, the Nernst−Einstein relation is violated under such conditions.[21] Experimental results from Calladine et al.[22] and Arvanitidou et al.[23] have shown that the low-field electrophoretic mobility of DNA molecules can decrease as fast as $\mu \sim 1/N^3$ for intermediate DNA sizes. Mayer et al.[24] found a $1/N^{1.6}$ dependence for small DNA molecules. More recently, Rousseau et al.[25] reported the results of a detailed study of the low field polyacrylamide gel electrophoresis of single-stranded DNA sequencing fragments. These authors observed regimes where $\mu \sim 1/N^{(1+\alpha)}$, with $0 \leq \alpha \leq 0.4$, when the field intensity was lower than about 30 V/cm and the gel concentration larger than about 3%. High gel concentrations and low field intensities are required to observe finite values of the exponent α. All of these results do not agree with the $1/N$ law predicted by the standard BRM.

However, entropic trapping of entire polymer chains in a large void is not the only possible explanations for the results reported above. Indeed, large values of α

S0024-9297(97)00763-8 CCC: $15.00
Published on Web 01/13/1998

were observed in ref 14 even when $R_g \gg \bar{a}$. Many authors have claimed that local interactions also play an important role in polyelectrolyte (such as DNA or sulfonated polystyrene) gel electrophoresis or polymer diffusion in quenched disordered media. In this article, we provide a mathematical approach to incorporate local interactions in the reptation model, a first step toward the development of a tube model that can tackle such questions.

Zimm and Lumpkin (ZL) recently developed a new reptation model to explain such anomalous reptative behavior.[26] These authors modeled the GE of macroions in an irregular matrix using a modified BRM where the chain interacts locally with the matrix. Their analysis indicated that the electrophoretic mobility does indeed decrease much faster than $1/N$ for intermediate-sized molecules if the local interaction are large enough. In the zero-field limit, ZL's analysis predicted that $D(N)$ becomes an exponential function of the molecular size N. In a subsequent article, Lumpkin[27] developed a different model describing the diffusion of the chain in a random matrix without external field as a discrete Ising-like jump process. His model predicts the usual reptation-like inverse-length dependence of the diffusion constant in the absence of a field.

The ZL model is a coarse-grained one which only considers chain hopping over length scales comparable to $h_x = \mathbf{h}\cdot\hat{\mathbf{E}}$, the component of end-to-end vector $\mathbf{h}$ of the chain in the field ($\mathbf{E}$) direction (x). Since it is not clear how to interpret the ZL model in terms of microscopic displacements of (mean) length $\bar{a}$, it is hard to determine which of the results are intrinsic to the model, and which might be an artifact of the coarse-graining procedure used in the calculation.

In the following sections, we develop a new mathematical approach, also based on the biased reptation model (but also valid in the zero field limit), to study the dynamics of long polymers in irregular matrices. We use stochastic equations for first-passage problems to calculate the exact expressions for the mean duration of the discrete jumps (of length $\bar{a}$) and the directional bias of these jumps in order to generalize the discrete reptation model of Doi and Edwards.[2] Our model differs from that proposed by Zimm and Lumpkin in that the distance migrated by the polymer during the "hopping process" is given by $\bar{a}$ (which is much smaller than h_x), the natural length scale of the reptation model. We then use our model to study the limit where the correlation length of the matrix energy parameter g is shorter than $\bar{a}$, such that the local energies associated with the reptation segments are uncorrelated (the limit originally studied by ZL). Our results are fundamentally different from those of ZL. Finally, we discuss different local energy models and their relevance for practical problems.

2. The Reptation Model

2.1. The Standard Reptation Model. The gel (or static gellike structure) in which the polymer migrates may be seen as a cage restricting the conformations the polymer can access. Indeed, the three-dimensional matrix formed by the gel fibers constitutes a set of topological constraints[1−5,13,28] that cannot be crossed by the polymer. A very long polymer can then be represented by a chain moving along the longitudinal axis of an imaginary tube. In practice, the polymer is modeled as a "primitive" chain of N effective "reptation segments" of length $\bar{a}$ which are not allowed to bend away from the tube axis. In the absence of electric forces ($E = 0$), the motion of a polymer is due solely to random thermal motion. The dynamics of the primitive chain in the standard reptation model is characterized by two assumptions: (a) the primitive chain and the tube have a constant contour length $L = N\bar{a}$; (b) the only allowed motion for a primitive chain is along the tube axis. We will keep these assumptions for our generalized reptation model. Thus, the motion of the primitive chain can be represented by a series of discrete displacements, or "jumps", of length $\bar{a}$ (Figure 1). A jump by the chain toward either end of the tube is equally probable due to the randomness induced by the thermal fluctuations and the (mean-field) homogeneity of the matrix. This is indeed the approach taken by Doi and Edwards in their seminal papers.[2−5] Note that since the BRM reduces to the standard reptation model in the zero-field limit ($E \to 0$), the main predictions of the reptation model are given in the next section in terms of the BRM. For the same reason, the calculation of the new jumping rates and local biases (section 3) is done for the BRM, and the $E \to 0$ limit will be taken later when required.

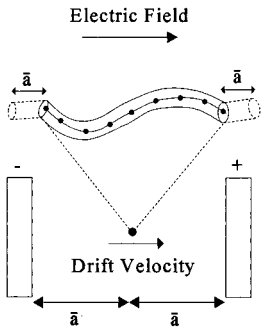

Figure 1. Tube model and its equivalent one-dimensional pointlike particle problem. An elementary jump of length $\bar{a}$ is completed when the particle is absorbed by one of the walls.

2.2. The Biased Reptation Model. In the framework of the BRM, the electric field $\mathbf{E} = E\hat{\mathbf{x}}$ leads to a net force acting on the polyelectrolyte chain along its tube axis (the transverse component of the total force $Q\mathbf{E}$ plays no role because of the rigid-tube assumption). As shown by Slater, Rousseau and Noolandi,[29] the mean duration and the biased probability of a discrete "jump" of length $\bar{a}$ can be obtained by comparing the displacement of the chain in the tube to the diffusion of a particle halfway between two absorbing walls separated by a distance $2\bar{a}$ (Figure 1). The completion of a discrete jump by the chain simply corresponds to the absorption of the pointlike particle by one of the walls. In other words, the chain moves in its tube in response to Brownian motion (with a curvilinear diffusion constant $D_c \sim 1/N$, as in the Rouse model since the hydrodynamic interactions are screened by the gel) as well as to the field-induced drift (with an instantaneous curvilinear velocity $V_c \sim h_x E$). We replace this continuous motion by biased jumps of constant length $\bar{a}$. It is actually the lack of intratube degrees of freedom that allows us to replace the primitive chain by a pointlike object to determine its basic dynamical properties. However, one must keep track of the long-time memory effects that are typical of reptation dynamics, especially if a field is applied.

In the BRM, the probabilities of jumping toward the $\pm$ end of the tube (the $+$ and $-$ ends are defined

arbitrarily; see Figure 1) are given by[29]

$$p_{\pm}(h_x) = \frac{1}{1 + \exp[\mp 2\delta(h_x)]} \tag{1}$$

where the conformation-dependent bias factor $\delta(h_x)$ is given by

$$\delta(h_x) = \epsilon \frac{h_x}{\bar{a}} \tag{2}$$

and the scaled electric field intensity ϵ is defined as

$$\epsilon = \frac{qE\bar{a}}{2k_B T} \tag{3}$$

with $q = Q/N$ being the electric charge of one reptation segment. The mean first-passage time required to jump over a distance $\bar{a}$ (in either direction) is given by[29]

$$\frac{t_{\pm}(h_x)}{\tau_B} = \frac{\tanh[\delta(h_x)]}{\delta(h_x)} \tag{4}$$

where $\tau_B = \bar{a}^2/2D_c \sim N$ is the Brownian time necessary for the diffusion of the chain over a curvilinear distance $\bar{a}$ when $\epsilon = 0$. The second moment is given by[21]

$$\frac{t_{\pm}^2(h_x)}{\tau_B^2} = \frac{1}{\delta^2(h_x)}\left[\tanh^2[\delta(h_x)] - \operatorname{sech}^2[\delta(h_x)] + \frac{\tanh[\delta(h_x)]}{\delta(h_x)}\right] \tag{5}$$

The probability that the new (jumping) end-segment will assume a new orientation $\Theta(t)$ between Θ and $\Theta + d\Theta$ ($0 \le \Theta \le \pi$) with the field axis is[18,29]

$$P(\Theta)\, d\Theta = \frac{1}{2}\frac{\epsilon}{\sinh(\epsilon)} \sin(\Theta)\, d\Theta\, e^{\epsilon \cos(\Theta)} \tag{6}$$

We note that if the field is turned off ($\epsilon = 0$), we obtain $P(\Theta)\, d\Theta = {}^1/_2\, d[\cos(\Theta)]$, as expected for an isotropic system.[18,29] Using these equations, we can model polyelectrolyte GE (for $\epsilon > 0$) or normal reptation (for $\epsilon = 0$) using computer simulations or analytical calculations.

Let us now review some of the fundamental analytical results of the reptation model. In the zero-field limit ($\epsilon \to 0$), we can calculate the diffusion coefficient using the Doi and Edwards approach[2] to obtain

$$D(N,\epsilon\to 0) = \lim_{t\to\infty} \frac{\langle [R_{cm}(t) - R_{cm}(0)]^2 \rangle}{6t} = \frac{D_c}{3(N+1)} \sim \frac{1}{N(N+1)} \tag{7}$$

where $R_{cm}(t)$ is the position of the center of mass at time t and $D_c = \bar{a}^2/2\tau_B \sim N^{-1}$. (Note that the result $D \sim (4N + 1)/(4N^2)$ found in ref 2 is incorrect due to several minor mistakes in the derivation.) For low field intensities ($0 < \epsilon < 1$), approximate analytical expressions for the electrophoretic velocity $V(N,\epsilon)$ and the diffusion coefficient $D(N,\epsilon)$ can be obtained from the BRM. The velocity first decreases like $1/N$, then goes through a shallow minimum, and finally reaches a plateau value for large molecular sizes N. More precisely, one gets the following scaling laws:[18,21,29]

$$\begin{aligned} V(N,\epsilon) &\cong \frac{\bar{a}}{\tau_B}\frac{\epsilon}{3} \sim N^{-1}E, && N\epsilon^2 < 1 \\ &= \text{shallow minimum}, && N = N_{min} \cong 14/\epsilon^2 \\ &\cong \frac{\bar{a}}{\tau_B}\frac{N\epsilon^3}{9} \sim N^0 E^3, && N\epsilon^2 \gg 14 \end{aligned} \tag{8}$$

The diffusion coefficient (in the field direction) decreases successively like N^{-2} and $N^{-1/2}$, goes through a broad maximum, and finally reaches a plateau value for large molecular sizes. A detailed analysis of the BRM demonstrates that the relevant scaling laws are[21]

$$\begin{aligned} D(N,\epsilon) &\cong D_c\frac{1}{3(N+1)} \sim N^{-2}\, E^0, && N < N_d \equiv 1.68\,\epsilon^{-2/3} \\ &\cong D_c\frac{\epsilon\sqrt{2N}}{3\sqrt{3\pi}} \sim N^{-1/2}\, E, && N_d < N < \epsilon^{-2} \\ &\cong D_c\frac{N\epsilon^2}{9} \sim N^0\, E^2, && N > \epsilon^{-2} \\ &= \text{broad maximum}, && N = N_{max} \cong 28\,\epsilon^{-2} \cong 2N_{min} \end{aligned} \tag{9}$$

The BRM thus predicts that the nonlinear effects invalidate the Nernst−Einstein relation when $N > N_d \cong \epsilon^{-2/3}$, i.e. before the mobility is affected (which occurs only for $N > \epsilon^{-2} > N_d$).

Note that it was recognized a few years ago that the orientation process assumed by the biased-reptation model is not appropriate for flexible polyelectrolytes. For the latter, the orientation term used in the BRM is indeed dominated by another term arising from the coupling between the fast fluctuations in the chain end's (curvilinear) positions and the local chain orientation. The resulting model is called the biased reptation with fluctuations (BRF) model.[30−32] In this article, we follow the original BRM in order to compare our finite-field results with those obtained by Zimm and Lumpkin. The effects of the fluctuations (for flexible polyelectrolytes) and orientation coupling (for stiff polyelectrolytes) are left for future investigations.

2.3. The Random Fluctuation Model. In the reptation theory, each pore of the gel (i.e., each segment of the primitive chain) is assumed to be energetically equivalent. For certain applications, this assumption may actually be invalid. For instance, if the polymer moves in a narrow, curved space, either the macromolecule must bend, the gel must deform, or both must occur. Each of these cases requires energy and can lead to local energetic effects. Similarly, one may have direct interactions between the fibers and the segments of the polymer (e.g., random electric charges on the gel fibers may lead to local repulsive or attractive forces). As mentioned in section 1, local entropic effects may also affect the dynamics of long reptating polymers in inhomogeneous systems.

For the specific exemples treated in Section 4, we will closely follow the basic elements of the ZL local energy model[26]. We thus assume that the energy g_i (in units of $k_B T$) associated with pore i ($i = 1, ..., N$) remains fixed as long as a primitive segment occupies it. This assumption is probably valid for a stiff gel. We further assume that the correlation length of the matrix is

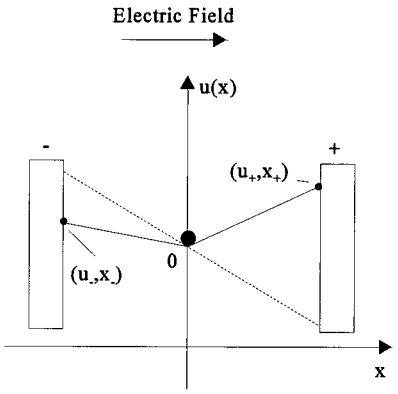

Figure 2. Pointlike particle in an external field and in the presence of disorder. The net potential $u(x)$ is shown for $g = 0$ (dashed line) and $g > 0$ (solid line). The walls are at $x_+ > 0$ and $x_- < 0$.

shorter than the segment length $\bar{a}$ of the reptation tube so that there is no correlation between the various g_i's. Note also that we implicitly treat an annealed gel since we keep no memory of the energy of a pore once the chain end segment has left it. The very interesting cases of quenched and correlated gels will be treated in another article. The distribution function $w(g_i)$ for the random local energies g_i is a Gaussian function with a zero mean and a standard deviation g

$$w(g_i) = \frac{1}{\sqrt{2\pi g^2}} \exp\left[-\frac{g_i^2}{2g^2}\right] \tag{10}$$

In practice, we cut the Gaussian beyond $2g$ in order to avoid exceedingly large trapping times. Note that the results do not depend strongly on the choice of the truncation cutoff because the distribution function decays very quickly for $g_i > 2g$.

As described previously, the motion of the chain inside the tube can be modeled as the diffusion of a particle between two absorbing walls (see Figure 1). The one-dimensional space of the particle problem is equivalent to the curvilinear tube axis (not the field axis). Thus, when the particle is absorbed by the + (or −) "wall", the chain has effectively completed a jump toward the + (−) end of its tube (Figure 1). The effect of the electric field can be described in term of a longitudinal (or curvilinear) drift velocity, V_c, which can be obtained from a potential function U as $V_c = -\nabla U/\xi$, where $\xi \sim N$ is the curvilinear friction coefficient of the polymer. We can write this equation in terms of scaled variables such that $v_c = -\nabla u$ (with $v_c = V_c\tau_B/\bar{a}$ and $u = U/2k_BT$).

For a constant and uniform electric field (including $\epsilon = 0$), the effect of the local free energies g_i is represented as a random perturbation of the local (wall) potentials $u_\pm$ (Figure 2). The new values of $u_\pm$ are simply the sum of two terms: the electric potential ($\mp\delta$ defined in eq 2) and a random energy term. We can thus write

$$u_\pm = \mp\delta + \frac{\Delta g_\pm}{2} \tag{11}$$

where $\Delta g_\pm$ is the net change of the chain's total free energy $g_{tot} = \sum_i g_i$ during a jump of length $\bar{a}$ in the $\pm$ direction. Note that we assume the potential $u(x)$ to be linear between the initial position and the "wall" (Figure 2); this simplified assumption can easily be changed to study other models. When the chain completes a jump

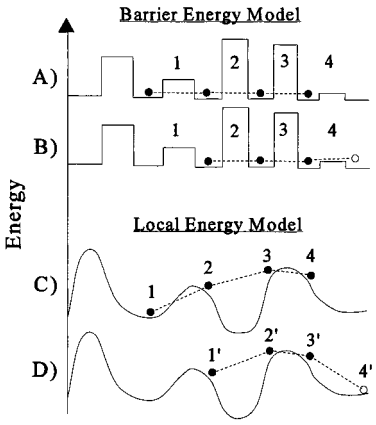

Figure 3. Two possible energy models. (A−B) A potential barrier of height g_i is present between each "pore" and the chain must overcome a potential barrier of total height $g_{tot}=\sum g_i \sim Ng$ in order to move. (C−D) The chain slides on a rough energy landscape. The change of energy when the chain moves over a distance $\bar{a}$ is given by $\Delta g = g(4') - g(1) \sim N^0 g$ here.

in the $\pm$ direction, the $\mp$ end tube segment disappears while a new tube segment is created at the $\pm$ end of the tube. Since all the internal chain segments slide, the net energy difference comes solely from the two ends (there is no net change in energy elsewhere along the chain). Therefore, $\Delta g_\pm$ is actually the difference in energy between the new tube section that is created and the old tube section that is destroyed, and we expect it to scale like $\Delta g_\pm \sim N^0$. This local energy model (Figure 3C) is clearly not a "barrier model" where each segment would have to overcome a local potential barrier (Figure 3A); in this situation, g_{tot} ($\sim N$) would actually be the energy $\Delta g_\pm$ required for the displacement of the polymer. In the barrier model, the chain thus requires much more energy than in the local energy model, and the different scaling laws for $\Delta g_\pm$ imply that the effect will be qualitatively as well as quantitatively different. In ZL's article,[26] the coarse-graining approximation effectively led to $\Delta g_\pm \sim N^{1/2}$; as we will see in section 4, this explains why our results differ.

The mean first-passage time and the probability that the particle (chain) will first reach a given wall (end of the tube) can be derived using stochastic methods (more precisely, the Fokker−Planck equation). We can also calculate the second moment of the first passage time to evaluate the diffusion coefficient of the polymer during the electrophoresis process with the same method. With these expressions, one can describe the details of the motion of a polyelectrolyte inside an irregular matrix during electrophoresis or in the absence of an electric field (normal diffusion).

2.4. First Passage Time Statistics. The Fokker−Planck equation[33] can be written as

$$\partial_t\, p(x,t|x',t') + \partial_x J(x,t|x',t') = 0 \tag{12}$$

where $p(x,t|x',t')$ is the (conditional) probability density that a particle will be at position x at time t given that it was at position x' at a previous time t'. The initial condition is simply

$$p(x,t'|x',t') = \delta(x - x') \tag{13}$$

The probability current for a stationary process, $J(x,t|x',t')$, is defined as

$$J(x,t|x',t') = A(x)p(x,t|x',t') - \frac{1}{2}\partial_x[B(x)p(x,t|x',t')] \quad (14)$$

where $A(x)$ is a drift velocity and $B(x)$ is a diffusion coefficient.

Let us now use the Fokker−Planck equation to study the dynamics of a particle initially at position x, such that $\alpha \le x \le \beta$. The total probability for this particle to exit through position α after time t is given by the time integral of the probability current at α. We thus define this probability by

$$p_\alpha(x,t) = -\int_t^\infty dt'\, J(\alpha,t'|x,0)$$

$$= \int_t^\infty dt' \left\{-A(\alpha)p(\alpha,t'|x,0) + \frac{1}{2}\partial_\alpha[B(\alpha)p(\alpha,t'|x,0)]\right\} \quad (15)$$

where the negative sign is needed since the current is to the left. Similarly

$$p_\beta(x,t) = \int_t^\infty dt' \left\{A(\beta)p(\beta,t'|x,0) - \frac{1}{2}\partial_\beta[B(\beta)p(\beta,t'|x,0)]\right\} \quad (16)$$

is the total probability for the particle to exit through β after time t. The probability that the particle exits at a time $T_\alpha > t$, given that it exits through α, is

$$\text{prob}(T_\alpha > t) = p_\alpha(x,t)/p_\alpha(x,0) \quad (17)$$

Since the system is stationary, we can write

$$p(\alpha,t|x,0) = p(\alpha,0|x,-t) \quad (18)$$

Using the fact that $p(\alpha,t|x,0)$ satisfies the backward Fokker−Planck equation,[33] we have

$$A(x)\partial_x p_\alpha(x,t) + \frac{1}{2}B(x)\partial_x{}^2 p_\alpha(x,t) = -\int_t^\infty dt'\, \partial_t, J(\alpha,t'|x,0) = J(\alpha,t|x,0) = \partial_t p_\alpha(x,t) \quad (19)$$

If $G(x,t)$ is the probability that $T \ge t$, the mean of any function of T is calculated as

$$\langle f(T)\rangle = -\int_0^\infty f(t)\, dG(x,t) \quad (20)$$

Thus, the mean exit time for a particle initially located at x, given that the exit is through α, is

$$\langle T(\alpha,x)\rangle = -\int_0^\infty t\, \partial_t\, \text{prob}(T_\alpha > t)\, dt = \int_0^\infty \frac{p_\alpha(x,t)}{p_\alpha(x,0)}\, dt \quad (21)$$

Integrating eq 19 with respect to t from 0 to ∞ results in

$$A(x)\partial_x[p_\alpha(x)\langle T(\alpha,x)\rangle] + \frac{1}{2}B(x)\partial_x{}^2[p_\alpha(x)\langle T(\alpha,x)\rangle] = -p_\alpha(x) \quad (22)$$

where we defined the probability of exit through α as $p_\alpha(x) = p_\alpha(x,0)$. The boundary conditions for this equation are straightforward since they follow from those of the backward Fokker−Planck equation, namely

$$p_\alpha(\alpha)\langle T(\alpha,\alpha)\rangle = p_\alpha(\beta)\,\langle T(\alpha,\beta)\rangle = 0 \quad (23)$$

In the first term, $\langle T(\alpha,\alpha)\rangle$ is zero (the time to reach α from α is zero) while in the second term, $p_\alpha(\beta)$ is zero (the probability of exiting through α, when starting from β, is zero). One can then solve eq 22 by using eq 21 for the mean exit time, given that the particle starting at x exits through α

$$\langle T(\alpha,x)\rangle = 2\left[\frac{1}{p_\alpha(x)}\int_x^\beta \frac{dy}{\psi(y)}\int_\alpha^y \frac{dy'\psi(y')p_\alpha(y')}{B(y')} - \int_\alpha^\beta \frac{dy}{\psi(y)}\int_\alpha^y \frac{dy'\psi(y')p_\alpha(y')}{B(y')}\right] \quad (24)$$

Similarly, the mean exit time, given that the particle starting at x exits through β is

$$\langle T(\beta,x)\rangle = 2\left[\int_\alpha^\beta \frac{dy}{\psi(y)}\int_\alpha^y \frac{dy'\psi(y')p_\beta(y')}{B(y')} - \frac{1}{p_\beta(x)}\int_\alpha^x \frac{dy}{\psi(y)}\int_\alpha^y \frac{dy'\psi(y')p_\beta(y')}{B(y')}\right] \quad (25)$$

where $\psi(y)$ is defined as

$$\psi(y) = \exp\left\{\int_\alpha^y dx' \frac{2A(x')}{B(x')}\right\} \quad (26)$$

One can also solve for the mean square exit time $\langle T^2\rangle$ using eqs 19 and 20 given that the particle initially located at x exits through α

$$\langle T^2(\alpha,x)\rangle = 4\left[\frac{1}{p_\alpha(x)}\int_x^\beta \frac{dy}{\psi(y)}\int_\alpha^y \frac{dy'\, p_\alpha(y')T(\alpha,y')\psi(y')}{B(y')} - \int_\alpha^\beta \frac{dy}{\psi(y)}\int_\alpha^y \frac{dy'\, p_\alpha(y')T(\alpha,y')\psi(y')}{B(y')}\right] \quad (27)$$

Similarly, if the exit is through β

$$\langle T^2(\beta,x)\rangle = 4\left[\frac{-1}{p_\beta(x)}\int_\alpha^x \frac{dy}{\psi(y)}\int_\alpha^y \frac{dy'\, p_\beta(y')T(\beta,y')\psi(y')}{B(y')} + \int_\alpha^\beta \frac{dy}{\psi(y)}\int_\alpha^y \frac{dy'\, p_\beta(y')T(\beta,y')\psi(y')}{B(y')}\right] \quad (28)$$

To calculate the probabilities of exiting through the two end-positions, we need the boundary conditions

$$p_\alpha(\alpha) = 1 \qquad p_\alpha(\beta) = 0 \quad (29)$$

as well as the normalization condition

$$p_\alpha(x) + p_\beta(x) = 1 \quad (30)$$

Equation 19 is to be solved in the limit $t \to 0$ (with $J(\alpha,0|x,0) = 0$ for $\alpha \ne x$). The probabilities that the particle will exit through $x = \alpha$ and $x = \beta$, respectively, are then given by

$$p_\alpha(x) = \frac{\int_x^\beta \frac{dy}{\psi(y)}}{\int_\alpha^\beta \frac{dy}{\psi(y)}} \qquad p_\beta(x) = \frac{\int_\alpha^x \frac{dy}{\psi(y)}}{\int_\alpha^\beta \frac{dy}{\psi(y)}} \quad (31)$$

Using the equations derived in this section, together with the BRM, we can now model the electrophoresis of polyelectrolytes and the normal reptation of polymers in irregular matrices.

These equations actually generalize the approach taken in ref 29. We can obtain the probability for jumping toward the ± end of the topological tube in a uniform electric field (or ±wall in our particle-between-walls analogy) from eqs 26 and 31 in terms of the scaled potentials $u_\pm$,

$$p_\pm \equiv p_{\pm 1}(0) = \frac{[e^{2u_\mp} - 1]}{\frac{u_\mp}{u_\pm}[e^{2u_\pm} - 1] + [e^{2u_\mp} - 1]} \qquad (32)$$

where $\alpha = -1$ and $\beta = 1$ (uniform pore sizes), the scaled drift coefficient is

$$\begin{aligned} a(x) &= u_- \qquad x \le 0 \\ &= -u_+ \qquad x \ge 0 \end{aligned} \qquad (33)$$

and the (uniform) scaled diffusion coefficient $b(x) = 2$. The equations for the mean first passage time $\langle T(\pm 1,0)\rangle/\tau_B$ and for $\langle T^2(\pm 1,0)\rangle/\tau_B{}^2$, which generalize eqs 4 and 5, are given in Appendix A for this particular limit.

For the case $g = 0$ ($u_\pm = \mp\delta$), eqs 1, 4 and 5 are recovered (where $t_\pm(h_x) = \langle T(\pm\bar{a},0)\rangle$ and $t_\pm{}^2(h_x) = \langle T^2(\pm\bar{a},0)\rangle$). Furthermore, for the case where $g = 0$ and $\alpha \neq -\beta$, we recover the equations derived by Rousseau.[34] Therefore, our equations are very general and reduce to all known special cases.

3. Methodology of the Simulations

In sections 3 and 4, we apply our generalized reptation equations to the specific random energy model described in section 2.3. We thus assume that the pores have a uniform size $\bar{a}$ (which implies that the tube has a constant length $N\bar{a}$). This model cannot be solved exactly if both the effects of the external field ϵ and the random interaction energies g_i are present. Therefore, our study will rely mostly on computer simulations. These simulations are very efficient, except for large values of g, since one then encounters very large jumping times $t_\pm$ which make it difficult to reach the steady-state. Because we use an annealed spatial energy distribution, the simulation does not have large memory requirements.

Since the polymer is assumed to take a random conformation when loaded into the gel during real diffusion or GE experiments, the chain is first created as a three-dimensional idealized freely-jointed random walk primitive chain where each step has a uniform length $\bar{a}$. In our simulation program and for the rest of this article, we use $\bar{a} = 1$ and $\tau_B(N = 1) = 1$ for the length and time scales (note that we then have $\tau_B(N) = N \times \tau_B(N = 1) = N$). An important aspect of this computer simulation is the absence of a predefined grid or lattice which would limit the chain motion to specific directions. Once the chain is created, with each segment energy g_i ($i = 1, 2, ..., N$) selected according to the distribution function eq 10, the following procedure is used to simulate the sequence of discrete jumps.

(a) First, we calculate the polymer's end-to-end distance, h_x, and the bias parameter $\delta = h_x\epsilon/\bar{a}$.

(b) Next, the random energies (noted g_0 and g_{N+1} at this stage) of the two possible new tube sections are generated (following the truncated Gaussian distribution function, eq 10). Following this, the values of $\Delta g_\pm$ are calculated as $\Delta g_+ = g_{N+1} - g_1$ and $\Delta g_- = g_0 - g_N$ since during a + (−) jump the $i = 1$ ($i = N$) tube segment will be lost while the $i = N + 1$ ($i = 0$) segment will be created. With δ and these values, we calculate the scaled potentials $u_\pm$ using eq 11.

(c) From the values of $u_\pm$, the probability of jumping toward the +end of the tube, p_+, is calculated using eq 32. We then compare p_+ with a random number between 0 and 1 to choose the curvilinear direction (+ or −) of the next step.

(d) Once the direction is known, we calculate the mean duration t_+ (or t_-) and the variance $\Delta t_+{}^2$ (or $\Delta t_-{}^2$) of the jumping process (see Appendix A) as well as the angular direction Θ of the new tube section (according to eq 6). Note that the angles Θ are assumed to be independent of the energies g_i.

(e) The chain is then moved in its tube in the selected (±) curvilinear direction. The current time is increased by $t_+ \pm \Delta t_+$ for a forward jump, or by $t_- \pm \Delta t_-$ for a backward jump (the ± in front of the standard deviation is selected randomly). We finally update the energy vector as well as the position vector.

This cycle is repeated until the steady-state is reached (this may require millions of iterations if g is large). Therefore, the simulation must be much longer than the transient period during which the chain explores the distribution of total energies g_{tot}. The duration of this transient period depends strongly on the local interaction energy parameter g. We then calculate the electrophoretic velocity V and/or the diffusion coefficient D (in the field direction) of the polymers as

$$V = \lim_{t\to\infty} \frac{d\langle x(t)\rangle}{dt}$$

$$D = \frac{1}{2}\lim_{t\to\infty} \frac{d}{dt}[\langle x^2(t)\rangle - \langle x(t)\rangle^2] = \frac{1}{2}\lim_{t\to\infty} \frac{d}{dt}\langle (x(t) - \langle x(t)\rangle)^2\rangle \qquad (34)$$

where the $\langle ...\rangle$ averages are over ensembles of identical molecules. The diffusion coefficient in the two transverse directions has not been studied. The diffusion coefficient can only be obtained if a large number of identical chains are simulated simultaneously. This consequence of the lack of self-averaging of D sometimes imposes a heavy burden on the simulations. It should be mentioned that the steady-state time t_{ssV} for V is shorter than that (t_{ssD}) for D (refer to Figures 4 and 5). The electrophoretic mobility μ is defined as $\mu = V/\epsilon$. The time, velocity, and diffusion coefficient are given in units of $\tau_B(N = 1)$, $\bar{a}/\tau_B(N = 1)$ and $\bar{a}^2/\tau_B(N = 1)$, respectively.

As an example, Figure 4 shows a log−log plot of the mean position $\langle x(t)\rangle$ vs time t for 1000 polymer molecules of size $N = 50$ with a field $\epsilon = 0.05$ and an energy parameter $g = 6.0$. After a transient period that extends to $t = t_{ssV} \simeq 10^8$, we find a slope of 1, indicating that a steady state has been reached. The steady-state velocity is $V = 5.57 \times 10^{-8}$. The gaps found for $t < 10^7$ are due to chains getting trapped in regions where the local energies are very low such that $t_\pm >> t$ (i.e. the jumping time exceeds the current time). A steady state is reached when the current time is larger than the longest jumping time $t_\pm(g)$ for the given system (in this case, the local free energy traps are renormalized to an

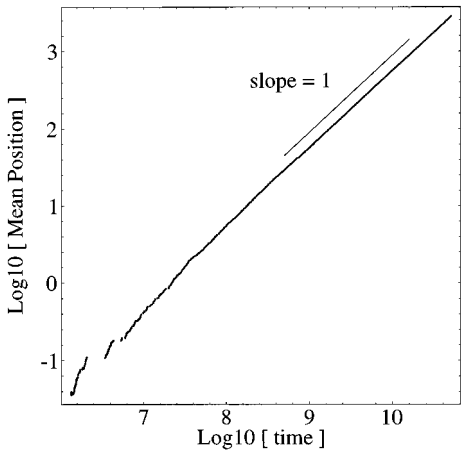

Figure 4. Mean position $\langle x \rangle$ vs time t for an ensemble of 1000 molecules. The parameters are $N = 50$, $\epsilon = 0.05$ and $g = 6.0$.

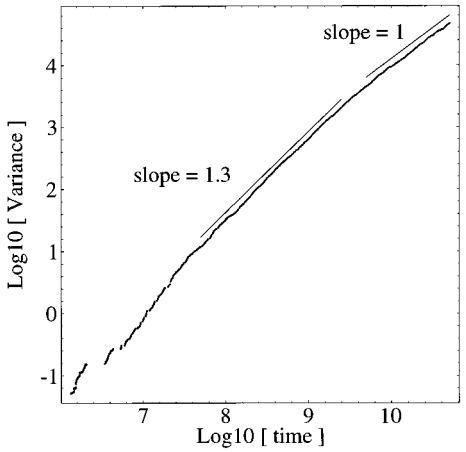

Figure 5. Variance $\langle \Delta x^2 \rangle$ as a function of time t, for the case described in Figure 4.

effective friction coefficient on such log−log plots). Figure 5 shows the variance $\langle \Delta x^2 \rangle \equiv \langle x^2 \rangle - \langle x \rangle^2$ vs time t for the same population of polymer molecules. The variance increases very quickly for times $t < 10^{9.5}$, which thus defines the diffusion steady-state time $t_{ssD} \approx 10^{9.5}$. For times $5 \times 10^7 < t < t_{ssD}$, we observe that $\langle \Delta x^2 \rangle \sim t^{1.3\pm0.1}$; this case of superdiffusion is due to the very broad distribution of jumping times $t_\pm$. Although the time dependence of the mean displacement and variance (or dispersion) during the short-time transient phases are interesting in themselves, they will not be studied in the following. For $t > t_{ssD}$, a slope of 1 is found and the steady-state diffusion coefficient is estimated to be $D_x = 4.55 \times 10^{-7}$ in this example. Note that since the angular directions Θ of the new tube sections are not coupled to the energies g_i, the conformational properties of our polyelectrolytes are identical to those predicted by the BRM.

4. Results

4.1. Testing the Algorithm. We first verify that our simulations, when used without local energies ($g = 0$), give the same results as the standard BRM.[21] The test results are shown in Figures 6 and 7, where the electrophoretic velocity V and the diffusion coefficient D are plotted against the number of segments (N) of the macroions for different scaled electric field intensities ϵ. One can clearly see that $V \sim \epsilon/N$ for small molecules, while the velocity plateaus to a value $V \simeq \epsilon^3/9$ for larger polymers. The behavior of the diffusion coefficient (in the field direction) shows three distinct regimes: for small molecules, we observe the zero-field value $D \sim 1/N(N+1)$; for large polymers, the diffusion coefficient D plateaus; between these two regions, the diffusion coefficient is first proportional to $\epsilon N^{-1/2}$ and then goes through a broad maximum. The points give the simulation results while the solid lines were obtained as described in Appendix B. There is good agreement between the simulation results and the numerical results of the approximate theoretical calculation[21] (solid lines), especially for low field intensities.

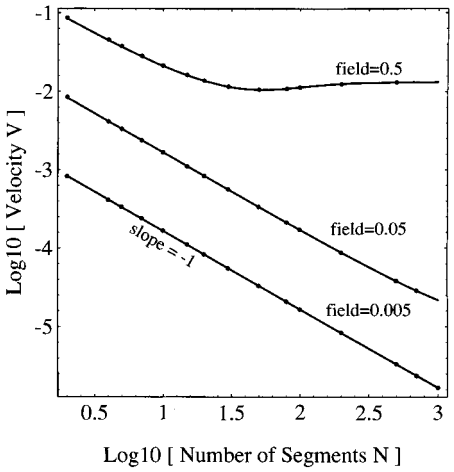

Figure 6. A log−log plot of the electrophoretic velocity V vs molecular size N for the $g = 0$ case. The solid lines come from the reptation theory (Appendix B), and the points are the results of computer simulations.

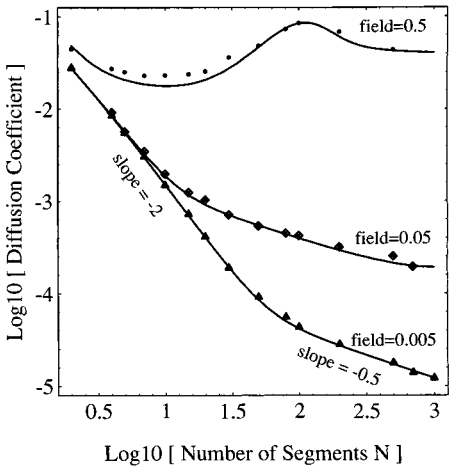

Figure 7. A log−log plot of the diffusion coefficient vs molecular size N for the $g = 0$ case. The solid lines come from the reptation theory (Appendix B), and the points are the results of computer simulations.

4.2. The Diffusion Coefficient in the Zero-Field Limit. In the absence of an electric field ($\epsilon = 0$), the motion of the polymer is solely due to the random thermal motion through the gel and we get $D(N,\epsilon = 0) \sim 1/N(N+1)$ for the tube model, as given by eq 7. When we take into account the effects of the local energy fluctuations, we find that the average first-passage time (eq A1 of Appendix A) required to jump over a distance $\bar{a}$ is given by

$$\frac{t_\pm(\epsilon \to 0)}{\tau_B} = \left(\frac{-1 + \exp(2\Delta g_\pm) - 2\Delta g_\pm}{2\Delta g_\pm^2} \right) \qquad (35)$$

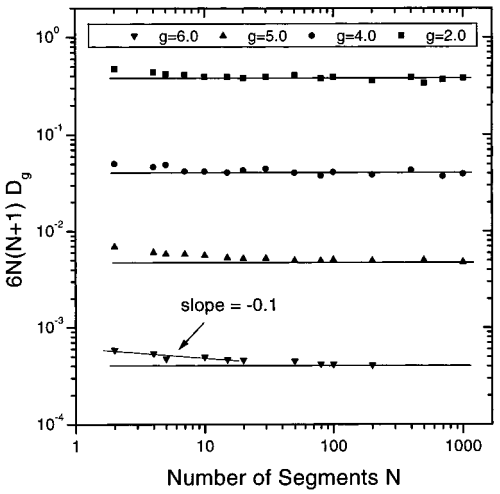

Figure 8. A log−log plot of the relative diffusion coefficient D_g*$6N(N+1)$ as a function of the molecular size N. Horizontal lines are shown to demonstrate that the scaling $D \sim 1/N(N+1)$ is conserved for long chains.

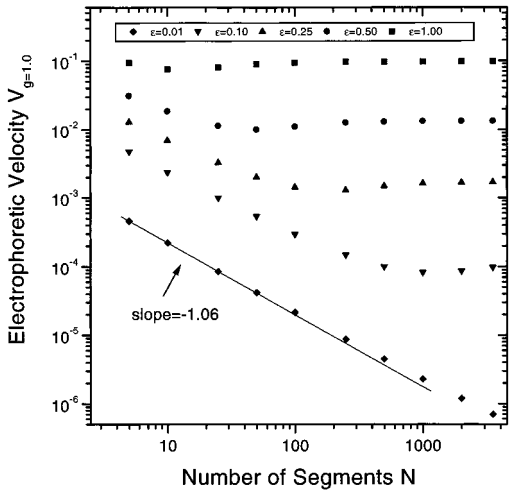

Figure 9. A log−log plot of the electrophoretic velocity V vs molecular size N for the $g = 1.0$ case.

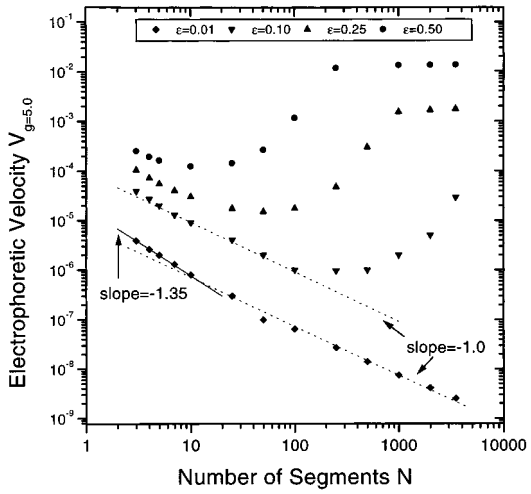

Figure 10. A log−log plot of the electrophoretic velocity V vs molecular size N for the $g = 5.0$ case.

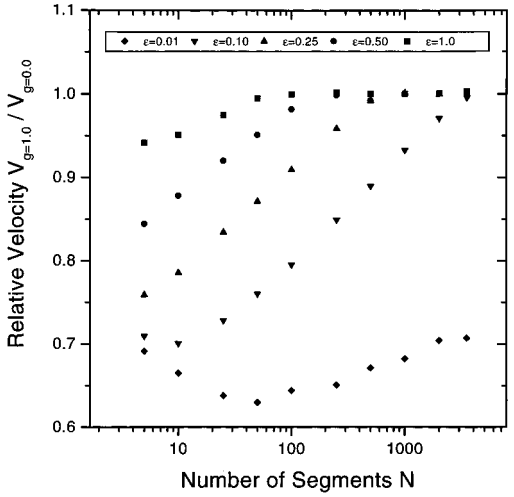

Figure 11. A semilog plot of the relative velocity $V_{g=1.0}/V_{g=0.0}$ vs molecular size N. The values of $V_{g=0.0}$ were calculated as described in Appendix B.

It is easy to show that $\langle t_{\pm}/\tau_B \rangle \geq 1.0$ for an unbiased distribution of energy differences $\Delta g_{\pm}$. Of course, this means that $D_g < D_{g=0}$. Figure 8 shows relative diffusion coefficient $D_g/D_{g=0}$ as a function of size N for $g = 2.0$, 4.0, 5.0, and 6.0. As we can see, the diffusion coefficient decreases very quickly when the energy parameter g increases. The $D \sim 1/N(N+1)$ scaling law appears to be preserved (in agreement with Lumpkin's model[27]), although small deviations are observed for short polymers. The range of these small deviations increases with g. These deviations comes from the fact that the local energies lead to correlated jumps of the chain (consecutive jumps in the same direction are less likely if $g > 0$), thus changing the scaling law for the tube disengagement time to $\tau \sim N^{3+\beta}$, with $\beta > 0$ (results not shown). This subtle effect of tube memory is lost if coarse-graining is used. We also note that this effect is found only for small molecular sizes and that the standard reptation scaling law $\tau \sim N^3$ is recovered for large sizes. The results found here are fundamentally different from those of Zimm and Lumpkin,[26] who observed that the N-dependence of the diffusion coefficient $D(N)$ changed from a power law to an exponential when g was increased. The main reason for this is related to the fact that our model describes the motion of a polymer chain in a system with uncorrelated annealed disorder. We believe that the results of ref 26 effectively correspond to correlated disorder with a correlation length $\lambda \approx |h_x|$ because of the mathematical method used by these authors. Here, the local energies effectively increase the viscosity of the environment and mainly reduce the magnitude of the diffusion coefficient.

4.3. The Electrophoretic Velocity in an Irregular Matrix. Figures 9 and 10 show log−log plots of the electrophoretic velocity V vs the size of the polymer (N), for energy parameters $g = 1.0$ and 5.0, respectively, as well as for different field intensities ϵ. Figures 11 and 12 give the corresponding relative electrophoretic velocities $V_g/V_{g=0}$. One of the main effects of the local free energies for low field intensities and/or small polyelectrolytes is a large decrease of the velocities. This can be explained by the fact that while the minimum duration for a jump is zero (e.g., if the local energies and net electric forces favor a quick jump), there is essentially no maximum when a polymer finds itself trapped in a region of the matrix where the local energies are low. When we increase the value of the local free energy parameter g, we increase the depth of these local traps and, consequently, we decrease the net electrophoretic velocity. For very large molecular sizes

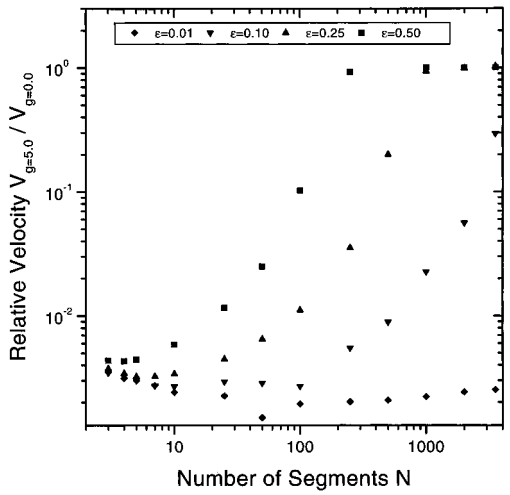

Figure 12. A log−log plot of the relative velocity $V_{g=5.0}/V_{g=0.0}$ vs molecular size N. The values of $V_{g=0.0}$ were calculated as described in Appendix B.

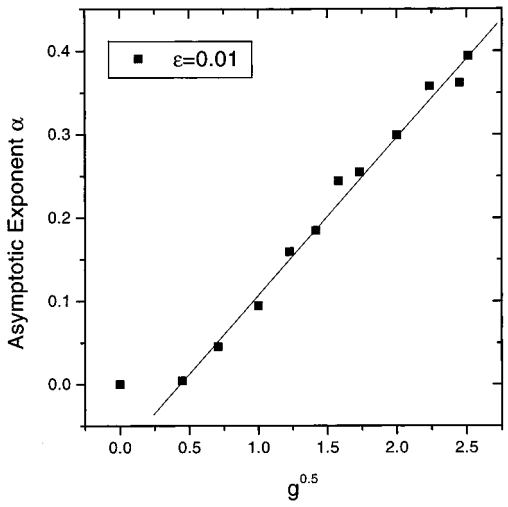

Figure 13. Asymptotic value of the exponent α vs the square-root of the energy parameter g.

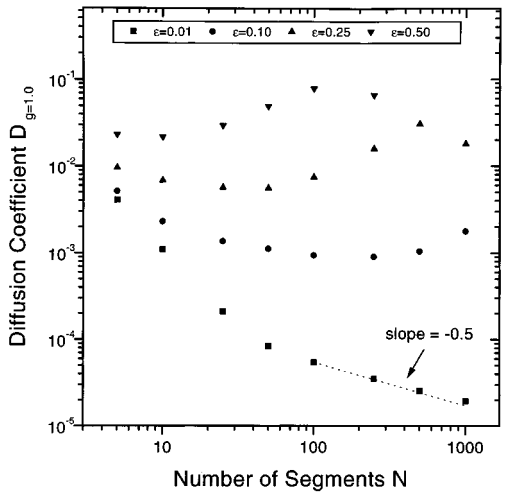

Figure 14. A log−log plot of the diffusion coefficient vs molecular size N for the $g = 1.0$ case.

N and/or electric field intensities ϵ, the ratio $V_g/V_{g=0}$ always reaches unity (Figures 11 and 12) because the electric forces then completely dominate the local energies g.

An understanding of the competition between the electric and interaction forces can be reached using simple scaling arguments. Short polymers ($N < 14/\epsilon^2 = N_{\min}$) remain unoriented and keep their random-walk statistics with $h_x \sim N^{1/2}$; this gives $u_\pm \approx \epsilon N^{1/2} + \Delta g_\pm/2$, where $\Delta g_\pm \sim N^0 g$. If the first term dominates the second one in this expression, the random energies become irrelevant and the electrophoretic velocities reach normal ($g = 0$) values (Figures 11 and 12). The transition size N^* where both terms in $u_\pm$ are of equal magnitude is thus given by $N^* \sim (g/\epsilon)^2$, with the restriction that $N^* < N_{\min}$. Our data (Figures 11 and 12) confirm this scaling law and give $N^* \approx 2\,(g/\epsilon)^2$. This transition has a very important impact on the minimum mobility found at $N_{\min} = 14/\epsilon^2$ when $g = 0$. While the velocities remain unaffected for $N > N^*$, they decrease substantially for $N < N^*$. Since $N^* < N_{\min}$, this shifts the minimum mobility to a size $N_{\min}(g) < N_{\min}(g = 0)$. More importantly, however, this makes the minimum much deeper. This was also observed by Zimm and Lumpkin. As a consequence, it produces a very strong "band inversion", where larger polymers move much faster than smaller ones (see, e.g., Figure 10 for $\epsilon = 0.5$).

Another effect of the local free energies ($g > 0$) is that we now find the scaling law $V \sim N^{-(1+\alpha)}$, with $\alpha > 0$, for the electrophoretic velocity of small polyelectrolytes. In Figure 13, we have plotted the asymptotic exponent α defined by

$$\alpha = -\lim_{N\to 1}\left(\frac{\partial \log(V)}{\partial \log(N)} + 1\right) \tag{36}$$

as a function of $g^{0.5}$ for a low field intensity $\epsilon = 0.01$. Although $\alpha \approx 0$ when $g < 0.1$, we observe that $\alpha \sim g^{0.5}$ for large g's. In our simulations, the velocity, for small molecules, approaches a dependence as high as the −1.4 power of the length of the polymer for $N < 10$ ($\alpha \approx 0.4$). This effect comes from the fact that local energies change the scaling law for the tube disengagement time of small polymers as seen in section 4.2. Our result agrees with the experimental data obtained by Mayer et al. in polyacrylamide gels.[24] These authors found that the low-field (polyacrylamide gel) electrophoretic velocity can decrease as fast as $N^{-1.6}$ for small single-stranded DNA molecules (roughly for $N < 15$). Recent experimental results with single-stranded DNA also showed that at low fields one observes $V \sim N^{-(1+\alpha)}$, with α increasing linearly with the gel concentration.[25] As we can see in Figure 10, nonzero values of α can only be observed for low field intensities, in agreement with experimental data.[24,25]

The local free energies used in this model have important effects on small molecules whereas Zimm and Lumpkin found important effects for intermediate size polymers. The difference comes from the definition of the energy model; in the local free energy model, the difference between the free energy of two conformations scales as N^0 whereas in Zimm and Lumpkin's energy model, it is proportional to $N^{1/2}$. Since the electric forces are strictly proportional to $N^{1.0}$ for large values of $N\epsilon$ (oriented molecules), both models must converge toward the $g = 0$ limit for high field intensities and/or large molecular sizes. We do indeed observe this behavior for both models.

4.4. The Diffusion Coefficient in an Irregular Matrix. Figures 14 and 15 show log−log plots of the diffusion coefficient D vs the size N of the polyelectrolyte for different field intensities ϵ and for the energy

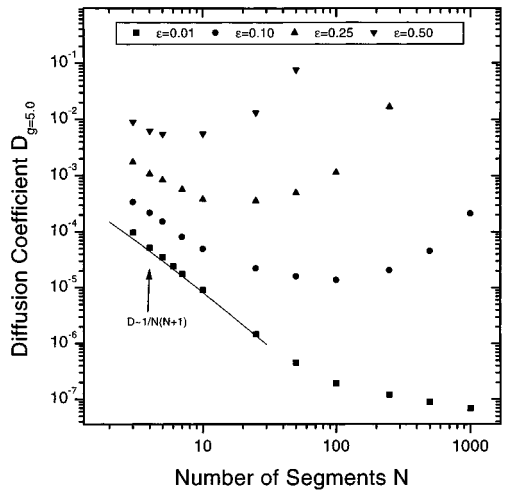

Figure 15. A log−log plot of the diffusion coefficient vs molecular size N for the $g = 5.0$ case. A line showing the scaling law of $1/N(N + 1)$ is provided for comparison.

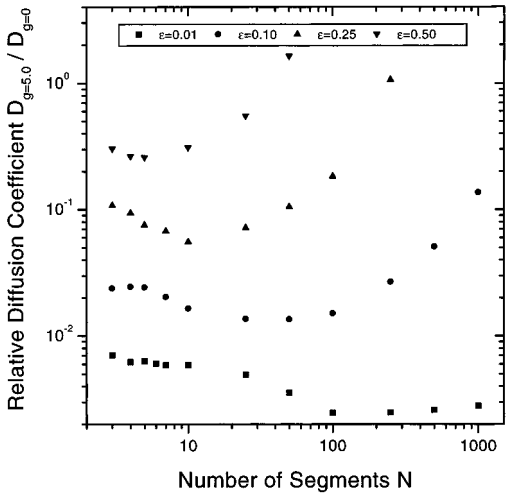

Figure 16. A log−log plot of the relative diffusion coefficient $D_{g=5.0}/D_{g=0.0}$ vs molecular size N. The values of $D_{g=0.0}$ were calculated as described in Appendix B.

distribution width set to $g = 1.0$ and 5.0, respectively. Figure 16 shows the relative diffusion coefficient $D_g/D_{g=0}$ as a function of the molecular size N for $g = 5.0$. (Note that we do not have data points for sizes larger than $N = 250$ for $\epsilon = 0.5$ since the steady state could not be reached in this case.)

In order to understand the diffusion results, we must keep in mind that in the presence of both an external field and disorder, diffusion is due to a combination of two different mechanisms. For low velocities, the diffusion coefficient is simply related to the mean rate $1/t_\pm$ at which the molecules jump. At high velocities, however, the atypically deep local traps play a large role, and the diffusion coefficient becomes proportional to $\Delta t_\pm^2/t_\pm^3$. This last regime can be derived as follows. If many molecules migrate together at high velocity ($t_\pm \ll 1$) and a few of them get trapped in a local (low-energy) environment where $t \approx t_\pm + \Delta t_\pm$, the latter will lag behind the group by a distance $\Delta x \sim v\Delta t_\pm$, hence giving a diffusion coefficient $D \sim \Delta x^2/t_\pm \sim \Delta t_\pm^2/t_\pm^3$.

For low field intensities, the local free energies diminish the diffusion coefficient because the mean jumping times increase exponentially with g (see section 4.2). Using the Nernst−Einstein relation $D_c = k_B T/\xi$

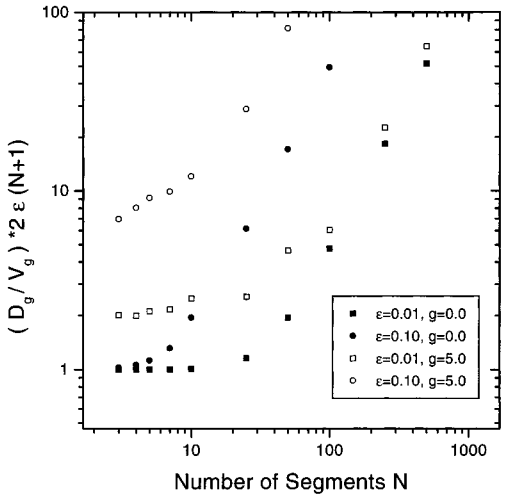

Figure 17. A log−log plot of the "Nernst−Einstein ratio" $(D_g/V_g)2\epsilon(N + 1)$ vs molecular size N for various cases.

or eqs 8 and 9 in the small N limit, we can relate the electrophoretic velocity to the diffusion coefficient to obtain the following relationship

$$D_g(N,\epsilon) = \frac{\bar{a}}{2\epsilon(N+1)} V_g(N,\epsilon) \tag{37}$$

Figure 17 shows a log−log plot of the "Nernst−Einstein ratio" $(D_g/V_g)2\epsilon(N + 1)$ vs molecular size N. When $g = 0$, the ratio is equal to unity for small molecular sizes, indicating that the Nernst−Einstein relation is valid in this limit. On the other hand, when $g > 0$, the ratio is always larger than unity.

Much like for velocities in the previous section, large molecules and/or large fields lead to situations where the electric forces dominate the local energies and the diffusion coefficients slowly converge toward their $g = 0$ values. Again, this leads to very deep minima (see Figure 15).

However, a new phenomenon is observed. In some cases (see Figure 16), the ratio $D_g/D_{g=0}$ actually exceeds unity. This surprising result is due to the mechanism explained above where the deep traps created by the g-energies increase the width $\Delta t_\pm$ of the distribution of jumping times. This increased width coupled to shorter mean times $t_\pm$ leads to enhanced dispersion of the molecules because $D \sim \Delta t_\pm^2/t_\pm^3$.

By comparing Figures 7 and 15, we also observed that higher field intensities increase the diffusion coefficient. Furthermore, the electric field dependence of the diffusion coefficient is much stronger when local free energies are present.

5. Conclusion

In this paper, we presented a mathematical model for the diffusion of polymers and the electrophoresis of polyelectrolytes in irregular matrices. Our model, which adds local free energies to the standard biased reptation model, actually provides a microscopic description of the model first proposed by Zimm and Lumpkin.[26] Using the theory of stochastic processes, we have calculated the basic parameters of the discrete random jumps carried out by the polymer chain in its reptation tube when an external field and/or local interaction energies are present. Our formulation of the problem allows us to study the subtle memory effects that are due to the reptation dynamics in the presence of local interactions.

The equations derived here can be used to study a variety of problems. For example, it would be quite interesting to study the diffusion of polymer chains in matrices where the random energies g are correlated over a distance $\lambda > \bar{a}$. For short chains such that $R_g < \lambda$, we expect the molecules to get trapped in local, low-energy volumes of size λ^3. For larger chains such that $R_g >> \lambda$, however, the chain is expected to effectively reptate in a "rough" tube. This could be a realistic model to study the effect of gel concentration inhomogeneities on polymer diffusion. In the presence of an electric field, further effects are expected when the electric forces orient short polymers and make them move quickly between low-energy areas.

As an example of application, we have looked at the local energy model studied by Zimm and Lumpkin.[26] Because the energy landscape is uncorrelated and annealed, the dynamics of the polymer is simply related to the change in free energy at the ends of the tube at each step. Therefore, the energy barrier affecting the basic reptation jumps (of length $\bar{a}$) scales like $\Delta g_{\pm} \sim gN^0$. In comparison, Zimm and Lumpkin's (ZL) coarse graining procedure led to jumps of length $|h_x| \sim N^{1/2}$ (for low fields). Not surprisingly, ZL's results show that even weak local interactions g can have dramatic effects on both the diffusion coefficient and the electrophoretic velocity. We believe that the coarse graining step effectively led to a system with a correlation length $\lambda \approx |h_x|$.

Our treatment of this model, on the other hand, keeps a strict correlation length $\lambda \approx \bar{a}$. In the absence of a field, our results predict a small increase of the molecular-size dependence of the diffusion coefficient. This comes from the fact that the local energies lead to correlated jumps of the chain in its tube (consecutive jumps in the same direction become less probable), thus changing the scaling law for the tube disengagement time to $\tau \sim N/D \sim N^{3+\beta}$, with $\beta > 0$. This subtle effect of tube memory is lost if coarse-graining is used. We also note that this effect is found only for small molecular sizes, and that the standard scaling law $D \sim N^{-2}$ is recovered very naturally for large molecular sizes. Our model thus predicts that deviations from the standard reptation model are expected only for small reptating molecules. Of course, the situation could be quite different with long-range correlations ($\lambda >> \bar{a}$) or quenched systems.

In the presence of an electric field, the situation can become quite complicated. For low fields and low molecular sizes, we simply get $V \sim N^{-1-\alpha}$, in agreement with some experimental results on the gel electrophoresis of polyelectrolytes.[22−25] For high fields, both the diffusion coefficient and the electrophoretic velocity converge toward their $g = 0$ values since the electric forces increase with molecular size while the effect of the local energies does not. The intermediate case is complicated and leads to very large mobility inversions, as found by ZL, and increased diffusion. Such effects have not been reported experimentally.

In conclusion, we have presented a set of generalized stochastic equations to study the reptation of polymer chains in the presence of local interaction energies. The example studied in this article provides interesting results that agree with some recent electrophoresis experimental data. Quenched and correlated systems along with the incorporation of the orientation factors predicted by the biased reptation with fluctuation (BRF) model represent the next logical step in this investigation of the effects of probe−matrix interactions in the reptation model.

Acknowledgment. This work was supported by FCAR and NSERC scholarships to S.J.H. and NSERC Research Grants to I.L. and G.W.S.

References and Notes

(1) de Gennes, P. G. *J. Chem. Phys.* **1971**, *55*, 572.
(2) Doi, M.; Edwards, S. F. *J. Chem. Soc., Faraday Trans 2* **1978**, *74*, 1789.
(3) Doi, M.; Edwards, S. F. *J. Chem. Soc., Faraday Trans 2* **1978**, *74*, 1802.
(4) Doi, M.; Edwards, S. F. *J. Chem. Soc., Faraday Trans 2* **1978**, *74*, 1818.
(5) Doi, M.; Edwards, S. F. *J. Chem. Soc., Faraday Trans 2* **1978**, *75*, 38.
(6) Klein, J. *Nature* **1978**, *271*, 143.
(7) Kremer, K.; Grest, G. S. *J. Chem. Phys.* **1994**, *92*, 5057.
(8) Rotstein, N. A.; Lodge, T. P. *Macromolecules* **1992**, *25*, 1316.
(9) Baumgärtner, A.; Muthukumar, M. *J. Chem. Phys.* **1987**, *87*, 3082.
(10) Muthukumar, M.; Baumgärtner, A. *Macromolecules* **1989**, *22*, 1937.
(11) Zimm, B. H. *Electrophoresis* **1996**, *17*, 996.
(12) Bouchaud, J. P.; Georges A. *Phys. Rep.* **1990**, *195*, 127.
(13) Baumgärtner, A.; Muthukumar, M. In *Advances in Chemical Physics, Polymeric Systems*; Prigogine, I., Rice, S. A., Eds.; John Willey & Sons, Inc., New York, 1996; p 625.
(14) Slater, G. W.; Wu, S. Y. *Phys. Rev. Lett.* **1995**, *75*, 164.
(15) Zimm, B. H. *J. Chem. Phys.* **1991**, *94*, 2187.
(16) Disch, C.;. Loomans, D.; Sokolov, I. M.; Blumen, A. *Electrophoresis* **1996**, *17*, 1060.
(17) Ogston, A. G. *Trans. Faraday Soc.* **1958**, *54*, 1754.
(18) Lumpkin, O. J.; Déjardin, P.; Zimm, B. H. *Biopolymers* **1985**, *24*, 1573.
(19) Noolandi, J.; Rousseau, J.; Slater, G. W.; Turmel, C.; Lalande, M. *Phys. Rev. Lett.* **1987**, *58*, 2428.
(20) Duke, T. A. J.; Semenov A. N.; Viovy, J. L. *Phys. Rev. Lett.* **1992**, *69*, 3260.
(21) Slater, G. W. *Electrophoresis* **1993**, *14*, 1.
(22) Calladine, C. R.; Collis, C. M.; Drew, H. R.; Mott, M. R. *J. Mol. Biol.* **1991**, *221*, 981.
(23) Arvanitidou, E.; Hoagland, D. *Phys. Rev. Lett.* **1991**, *67*, 1464.
(24) Mayer, P.; Slater, G. W.; Drouin, G. *Appl. Theor. Electrophor.* **1993**, *3*, 147.
(25) Rousseau, J.; Drouin, G.; Slater, G. W. *Phys. Rev. Lett.* **1997**, *79*, 1945.
(26) Zimm, B. H.; Lumpkin, O. *Macromolecules* **1993**, *26*, 226.
(27) Lumpkin, O. *Phys. Rev. E* **1993**, *48*, 1910.
(28) Doi, M.; Edwards, S. F. *The Theory of Polymer Dynamics*, Oxford University Press: NewYork, 1986.
(29) Slater, G. W.; Rousseau, J.; Noolandi, J. *Biopolymer* **1987**, *26*, 863.
(30) Duke, T. A. J.; Semenov, A. N.; Viovy, J. L. *Phys. Rev. Lett.* **1992**, *69*, 3260.
(31) Duke, T. A. J.; Viovy, J. L.; Semenov, A. N. *Biopolymers* **1994**, *34*, 239.
(32) Semenov, A. N.; Duke, T. A. J.; Viovy, J. L. *Phys. Rev. E* **1995**, *51*, 1520.
(33) Gardiner, C. W. *Handbook of Stochastic Methods*, Springer-Verlag: Berlin, 1985.
(34) Rousseau, J. M.Sc. Thesis, University of Waterloo, Waterloo, Canada, 1988.

Appendix A: Mean Duration and Variance of the Jumps

The equation for the mean scaled first passage time can be derived using eqs 24, 25, 26, 27, 28, 31, and 33. For the special case where $\alpha = -\beta = -1$ (uniform pore sizes) and $b(x) = 1$ (uniform diffusion coefficient), the average duration (first moment) of a jump is given by

$$t_\pm = \langle T(\pm 1,0)\rangle = \frac{2FEGu_\pm^2 + 2u_\mp u_\pm(u_\pm(C(4 - C - 2D) - 1) - FE^2) - u_\mp^2(2E(2F + u_\pm(1 + D)))}{u_\pm^2 u_\mp E(Eu_\pm + Fu_\mp)}\tau_B \quad \text{(A1)}$$

where we have defined the following parameters to simplify the result: $C = \exp(u_-)$, $D = \exp(u_\pm)$, $E = 1 - C$, $F = 1 - D$ and $G = 1 + C$. The second moment of the first passage time is given by

$$\begin{aligned} t_\pm^2 = \langle T^2(\pm 1,0)\rangle = [&8E^2FGu_\pm^5 + \\ &u_\mp(8EFu_\pm^4(2Cu_\pm - FG(C + 2)) + \\ &u_\mp(8u_\pm^3(-2DE^2FG + \\ &u_\pm(1 + D(-3 + C(7 - 2D(1 + 2C) + \\ &C(11 - 3C))) + C(-3 + C(C - 5)) + 2CFGu_\pm)) + \\ &u_\mp(4u_\pm^2(2EF(4 - 2CE + D(C(C - 4) - 1)) + \\ &u_\pm(-2E(D(D - 3) - 1 + C(D(10 - 3D - 3C) - 1)) + \\ &u_\pm(C(11 + C(C - 7)) - 1 + 4CD(D + 3C - 5)))) + \\ &u_\mp(8u_\pm(E^2F(5 + D) + u_\pm(D(D + 6) - 1 + \\ &C(6 - C) + CD(2D + 6C + CD - 20) + \\ &u_\pm(C(4 - C) - 1 + D(C(6 - 2D - 3C) - 3)))) + \\ &u_\mp(4E(-4F^2 + u_\pm(2F(1 + D) + \\ &u_\pm(1 + D(D + 6)))))))))]t_B^2/[Eu_\pm^4u_\mp^3(Fu_\mp + Eu_\pm)^2] \end{aligned} \quad \text{(A2)}$$

The variance of the first passage time is simply given by

$$\Delta t^2 = t_\pm^2 - (t_\pm)^2 \quad \text{(A3)}$$

Appendix B: Electrophoretic Velocity and Diffusion Coefficient

Approximate values for the electrophoretic velocity V and the diffusion coefficient D can be calculated numerically using the theoretical approach described in ref 21. For instance, the following relation provides an excellent approximation for V:

$$\mathrm{V(N,\epsilon)} \cong \frac{\bar{a}}{\mathrm{N}\epsilon\tau_B}\frac{\langle\delta\tanh(\delta)\rangle}{\langle\delta^{-1}\tanh(\delta)\rangle} \quad \text{(B1)}$$

The $\langle ...\rangle$ averages here are over a biased Gaussian distribution function for the end-to-end distances h_x.[21] The following *Mathematica* program was used to generate the solid curves of Figure 6:

```
ReptationMu[n_,e_] :=
    Module[{kos, kos2, sigma2, gaussian, delta, deltamax, deltawidth},
                kos=Coth[e]-1/e; kos2=1-(2*kos)/e; sigma2=kos2 - kos^2;
                deltamax=n*e*kos; deltawidth=2*n*sigma2*e^2;
                gaussian[delta_]:= Exp[-(delta-deltamax)^2 / deltawidth];
                ave[f_] := NIntegrate[f*gaussian[delta],{delta, -Infinity, 0, Infinity},
                                MinRecursion->5, MaxRecursion->30];
                ave[delta*Tanh[delta]]/(n^2 * e^2 * ave[Tanh[delta]/delta])
        ]
```

The theoretical expression for the diffusion coefficient $D(N,\epsilon)$ is less precise than that for the velocity. The diffusion coefficient is given by a sum of two terms, $D(N,\epsilon) = D_T(N,\epsilon) + D_{\Delta T}(N,\epsilon)$, where $D_T(N,\epsilon)$ correspond to the standard thermal diffusion

$$D_T(N,\epsilon) \cong \frac{\bar{a}^2\sigma^2}{2(N + 1)\tau_B}\langle N\delta\tanh(N\delta)^{-1}\rangle \quad \text{(B2)}$$

where $\sigma^2 = (\langle\cos^2\theta\rangle - \langle\cos\theta\rangle^2)$ is the variance of the average tube segment projection (calculated using eq 6). $D_{\Delta T}(N,\epsilon)$, the component due to the width of the distribution of jumping times, is given by

$$\mathrm{D_{\Delta T}(N,\epsilon)} \cong \frac{\bar{a}^2}{\tau_B}\cdot\frac{1}{N\epsilon^2}\cdot\frac{\langle\delta\tanh(\delta)\rangle^2}{\langle\tanh(\delta)/\delta\rangle^3}\left[\left\langle\left(\frac{\tanh(\delta)}{\delta}\right)^2\right\rangle - \left\langle\left(\frac{\tanh(\delta)}{\delta}\right)\right\rangle^2\right] \quad \text{(B3)}$$

The following *Mathematica* program has been used to calculate the diffusion coefficient (solid curves) in Figure 7:

```
ReptationDx[n_,e_] :=
    Module[{kos,kos2,deltamax,sigma2,deltawidth,ave,f,delta,spdw,
                        term1,term2,term3,term4},
            kos=Coth[e] - 1/e;  kos2=1 - (2*kos)/e; sigma2=kos2 - kos^2;
            deltamax=n*e*kos; deltawidth=2*n*sigma2*e^2;
            spdw=Sqrt[Pi*deltawidth];
            ave[f_] := NIntegrate[f*Exp[-((delta - deltamax)^2/deltawidth)]/spdw,
                        {delta, -Infinity, 0, Infinity},
                        MinRecursion->5, MaxRecursion->30];
            term1=ave[delta * Tanh[delta]];
            term2=ave[Tanh[delta]/delta];
            term3=ave[(Tanh[delta]/delta)^2];
            term4=ave[n*delta/Tanh[n*delta]]/(n+1);
            (sigma2*term4+2*term1^2*(term3/term2^2-1) / (e^2* term2*n)) /
                        (2*n)
    ]
```

For example, for a molecular size $n = 10$ and a field intensity $e = 0.10$, we obtain:

```
In[1] := {ReptationMu[10,0.10],ReptationDx[10,0.10]}

Out[1] := {0.0336401,0.00271372}
```

MA970763F